Simple On-Line X-Ray Setup to Monitor Structural Changes During Fiber Processing

BENJAMIN S. HSIAO,[1] RANDOLPH BARTON, JR.,[1,*] and JOHN QUINTANA[2]

[1]DuPont Central Research & Development, Experimental Station, Wilmington, Delaware 19880, and [2]DND-CAT, Advanced Photon Source, Argonne National Laboratory, Argonne, Illinois 60439

SYNOPSIS

We demonstrate that on-line X-ray characterization during fiber processing can be carried out using a low-power X-ray generator and an image plate detector. Two fiber processes using 66-nylon were chosen as examples: high-temperature drawing at different ratios (3.5–5.0 X) and melt spinning at moderate speeds (450 and 1,200 mpm). For the draw measurement, useful diffraction images were obtained in a reasonable time frame (30 min). These patterns were equal in quality to static in-laboratory images and sufficient for quantitative analysis. Results showed significant differences in structure between on-line and off-package samples. The crystal density was found to be lower but the crystal orientation was found to be higher as draw ratio increases. The on-line spinning image was found to be similar to those obtained by synchrotron X-ray measurements, which confirm the development of two-dimensional crystals having a hydrogen bonding characteristic distance during spinning. Finally, several ways to improve the demonstrated on-line setup design will be discussed. © 1996 John Wiley & Sons, Inc.

INTRODUCTION

In industrial fiber research, X-ray diffraction is an important tool for characterizing structural information such as unit cell parameters, crystal orientation, crystallinity (index), and crystallite size.[1,2] In spite of the increasing need for using on-line techniques to improve the yield and uniformity of products and processes, X-ray measurements are nearly always made on finished yarns, i.e., samples removed from a wound-up package. This is in sharp contrast to the many successful on-line X-ray studies demonstrated during fiber processing.[3–11] Perhaps the primary difficulties in applying conventional X-ray technology in a real process are the limitations of the X-ray film and electronic detection technology. The former requires a long exposure time (several hours) as well as elaborate procedures to extract data for quantitative analysis. The latter involves bulky size restrictions and delicate electronics that are not robust under harsh fiber-processing conditions.

The recent development of new X-ray detection technology, namely, the display phosphors technology, has practically resolved these problems. The two major classes of X-ray detectors based on the technology, image plate,[12–15] and charge-coupled device (CCD) camera[16–18] (for examples) have a sensitivity about 10–100 times better than that of X-ray films.[12–18] The improved sensitivity enables the collection of high-quality X-ray images in shorter time (in minutes). Furthermore, all images are readily readable in a digital form that eliminates the need for digitization from film negatives. In this study, we will demonstrate a simple on-line X-ray characterization technique using a low-power X-ray generator and image plates to monitor structural changes during fiber processing. Two types of processes are chosen for this demonstration: 1) fiber drawing under different ratios at a high temperature, and 2) melt spinning under two moderate speeds (450 and 1,200 m/min). We will not consider the CCD technology here because it has restrictions similar to those of conventional electronic detectors. Finally, we will describe pos-

* To whom correspondence should be addressed.

Journal of Applied Polymer Science, Vol. 62, 2061–2068 (1996)
 CCC 0021-8995/96/122061-08

sible improvements to the current design which can be applied to virtually any fiber process.

EXPERIMENTAL

X-Ray Setup

The schematic diagram of the simple on-line X-ray apparatus is illustrated in Figure 1. In this study, measurements were in fact carried out in a slightly different setup but with similar design features. This setup utilized a standard transmission geometry with Ni-filtered Cu Kα radiation from a conventional AEG Cu X-ray sealed tube. The detection system consisted of a Fuji^{TM} HR-3 image plate (200 $\times$ 250 mm) enclosed in opaque plastic sheeting which was located 38 mm from the moving fiber. The wrapped image plate was mounted behind a lead-lined aluminum shield with a 90 mm^2 cutout detection window. This allowed us to take multiple images (four) on the same plate by moving an unexposed part of the plate into the detection window.

An incident beampipe defined the X-ray beam with a 0.5 mm pinhole located 165 mm from the X-ray target. Background radiation from the incident beampipe (e.g., fluorescence) as well as air along the incident beam path was minimized with a secondary scatter shield which slid along the beam pipe with a 2 mm pinhole at its end. This shield was brought directly up to the moving fiber, but not touching. Immediately after the fiber, a lead beamstop was used to catch the direct beam. This beamstop blocked the incident beam and the first 5° in 2θ out of the final pattern. A small bit of fluorescent powder was painted onto the beamstop to visually determine when the direct beam was blocked. The beamstop and secondary scatter shield on the beam pipe were found to be critical in eliminating background radiation which would otherwise fog the resultant pattern. While the Al mounting plate and X-ray tube were mounted to a motor-driven x-z stage to allow fine positioning relative to the fiber, we found it easier to position the fiber relative to the X-ray beam using a ceramic fiber guide. This guide was located approximately 5 mm downstream of the scattering position of the fiber. We believe that contact with the guide might alter the structure after but not prior to the contact.

A Fuji^{TM} BAS 2000 IP imaging plate scanner was used to obtain the digital image from each plate. Since the sensitivity of storage phosphors is typically 10 to 100 times higher than that of conventional X-ray film, we found that we could take acceptable

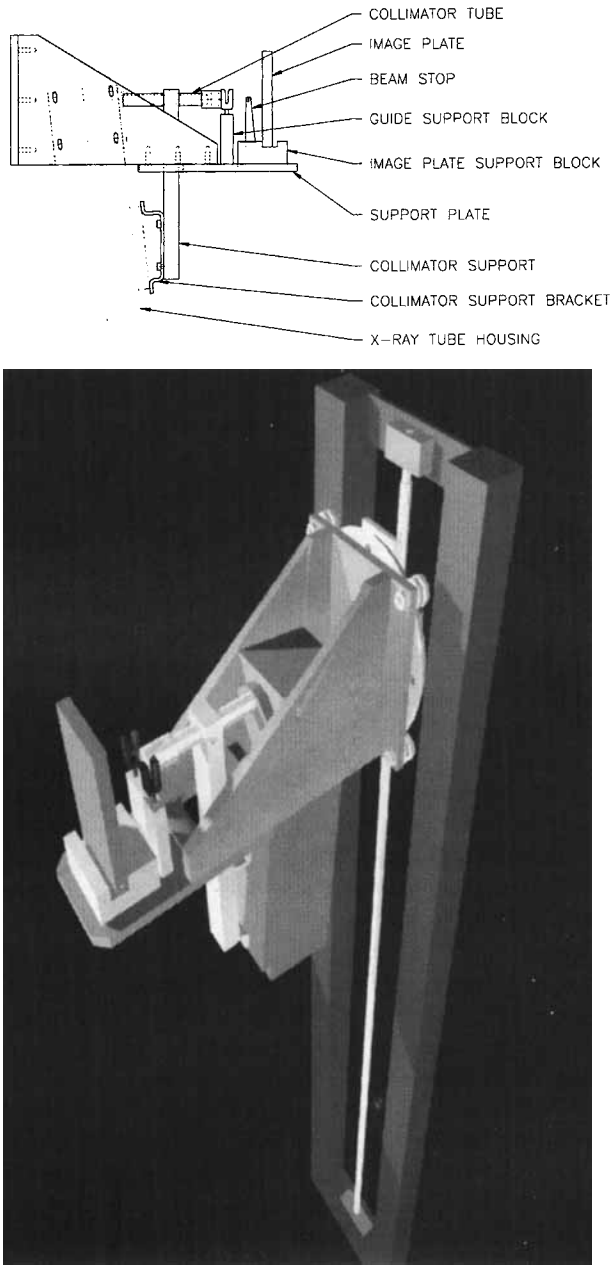

Figure 1 (a) Schematic diagram of on-line X-ray setup using low-power X-ray tube and imaging plate detector. (b) The three-dimensional cartoon of this setup.

images with 30 min exposures with the X-ray tube operating at about 1.4 kW (40 kV, 35 mA). A readout resolution of 100 μm was chosen during the scanning providing an intrinsic detector resolution of 0.15° on the image plate that was acceptable for quantitative analysis. The scanned intensity (IP) from the scanner was in a modified logarithmic scale and was subsequently converted to a real scale ($I = \exp(4*I_P/1023)$) for quantitative analysis.

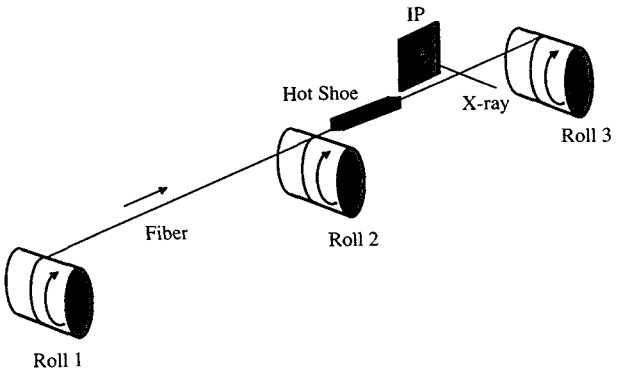

Figure 2 On-line X-ray detection during fiber-drawing measurement (processing variables in Table I).

Fibers and Processes

Drawing Experiment

Nylon 66 spun yarn consisting of 34 filaments with denier of 1,000 was used as the supply for low-speed two-stage drawing on-line measurements. The schematic diagram of the drawing experiment is illustrated in Figure 2. This setup contains three drawing rolls. The #1 and #2 rolls were separated by 1 m, and the #2 and #3 rolls were separated by 1.5 m. The X-ray detection spot was fixed at a position between rolls #2 and #3. Two arrangements were chosen for measurements: 1) the hot shoe (set at 200°C) was located between rolls #2 and #3, at a position ca. 20 cm before the X-ray detection spot; 2) the hot shoe (also set at 200°C) was placed between rolls #1 and #2. In the first case, the yarn temperature at the detection position is still close to draw temperature, although the precise value is not known; in the latter, the yarn was passed over roll #2 and essentially cooled to near room temperature. Three effective draw ratios were chosen: 3.50 ×, 4.25 × and 5.00 ×. The detailed processing variables during the drawing measurements are listed in Table I. The data collection time for each image was set at 30 min.

Spinning Experiment

Fiber yarn was spun from 42 RV (relative viscosity) nylon 66 flake using a single-screw extruder equipped with a 34-hole spinneret. The spinneret temperature was set at ca. 290°C, and the wind-up speed was operated at two different speeds: 450 and 1,200 m/min. The spun yarn had a denier of about 350 (34 filament). The X-ray detection was taken at about 4 m away from the spinneret, at which point the yarn has a temperature of about 50°C. The collection time for the image was 30 min.

RESULTS AND DISCUSSION

We will divide this section into two parts. The first part deals with the results from the two experiments, and the second part discusses possible improvements to the design and the points of caution for applying such an on-line technique.

On-Line Fiber Structural Characterization

Drawing Experiment

Figure 3 illustrates a typical collection of four images (after background subtraction) on a single image plate. These images include the calibration of nylon 66 monofilament (d-spacings of all reflections have been characterized by diffractometer), the control yarn with no drawing and no heat treatment, and two images from on-line detection under different draw ratios and temperatures. All of these images have acceptable quality, similar to static images obtained by two-dimensional gas-filled detectors in our laboratory.

Table I Processing Variables During Fiber-Drawing Measurements

Item	3.50×_HT	4.25×_HT	5.00×_HT	3.50×_LD	4.25×_LD	5.00×_LD
Roll#1 V (m/min)	7.2	7.2	7.2	7.5	7.5	7.5
Roll#2 V (m/min)	7.5	7.5	7.5	26.3	31.9	37.5
Roll#3 V (m/min)	26.3	31.9	37.5	26.1	31.5	37.1
Draw Ratio	3.50	4.25	5.00	3.50	4.25	5.00
Shoe Position	#2/#3	#2/#3	#2/#3	#1/#2	#1/#2	#1/#2
Shoe T (°C)	200	200	200	200	200	203
Tension In (g)	175	350	—	—	250	400
Tension Out (g)	200	280	—	—	250	350
Let-Down Tension (g)	—	—	—	100	100	170

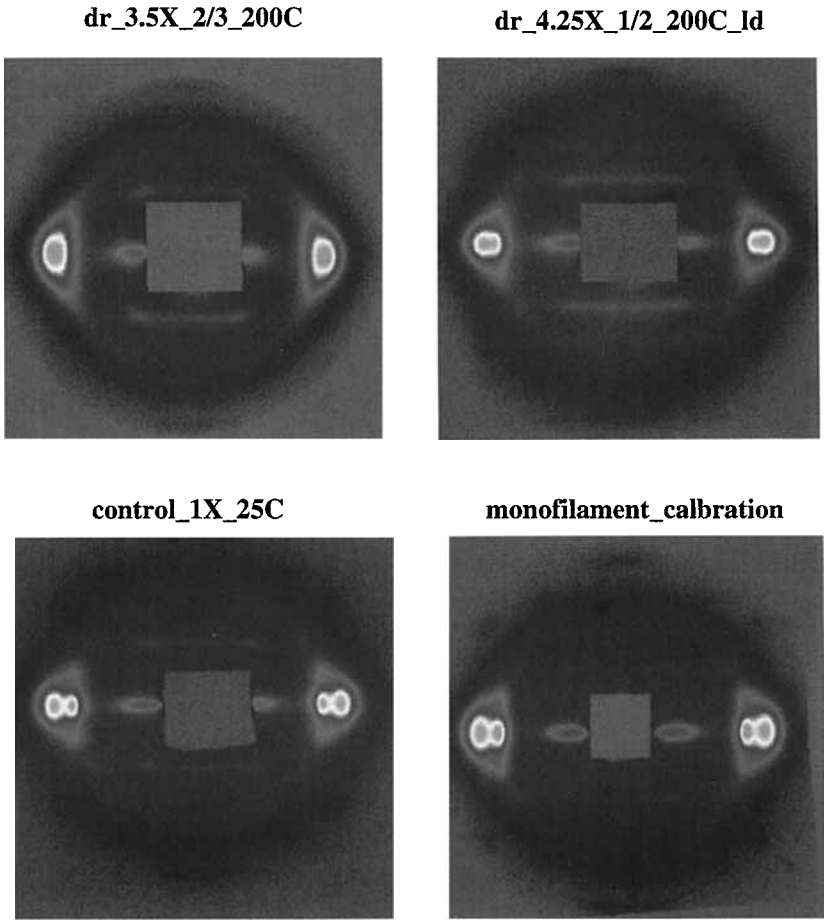

Figure 3 Typical two-dimensional WAXD images collected during on-line fiber-drawing experiments and from a calibrating fiber.

Visually, the major difference between the on-line images versus the control and calibration images is the appearance of the two strong reflections (100 and 010/110 doublet) on the equator. In the latter, the two peaks are well separated, while in the former, they are merging together, indicating the existence of a Brill transition-like behavior.[19] This behavior is seen in all of the observed on-line images. Several common features also are observed in all of the images. (1) An equatorial streak is always seen along the equator, which is due to the scattering by the sample from high-energy white radiation not completely absorbed by the nickel filter. (2) The appearance of the 002 and 015 layer lines persists, regardless of the changes in processing variables.

Hereafter, we will discuss only the analysis of equatorial scans; no analysis of meridional or off-axis reflections is carried out. Figures 4 and 5 illustrate the equatorial profiles from on-line wide-angle X-ray diffraction (WAXD) images under different processing conditions (they represent the high-tension (HT) and let-down (LD) series, respectively). It is found that at high temperatures (HT series, X-ray detector located ca. 10 cm from the hot shoe), a single reflection peak is observed at 4.25 × and 5.00 × draw ratios. However, as the ratio decreases to 3.50 ×, two reflections (indicated by two deconvoluted dashed lines) are seen. Since the temperature of the fiber at the detection spot under the three draw ratios is about constant, the increase in draw ratio appears to facilitate the occurrence of a single strong reflection on the equator. This single reflection is usually viewed as the triplet reflection peak (100/010/110) from the pseudohexagonal unit cell (in metric terms) above the Brill transition temperature (180°C for unoriented polymer), in contrast to a conventional triclinic cell[20] at room temperature. In a forthcoming study,[21] we will demonstrate that this single reflection is still a triclinic cell having a similar value in the *a*-axis (the interchain separation containing hydrogen bonding), but an increasing value in the *b*-axis and a decreasing value

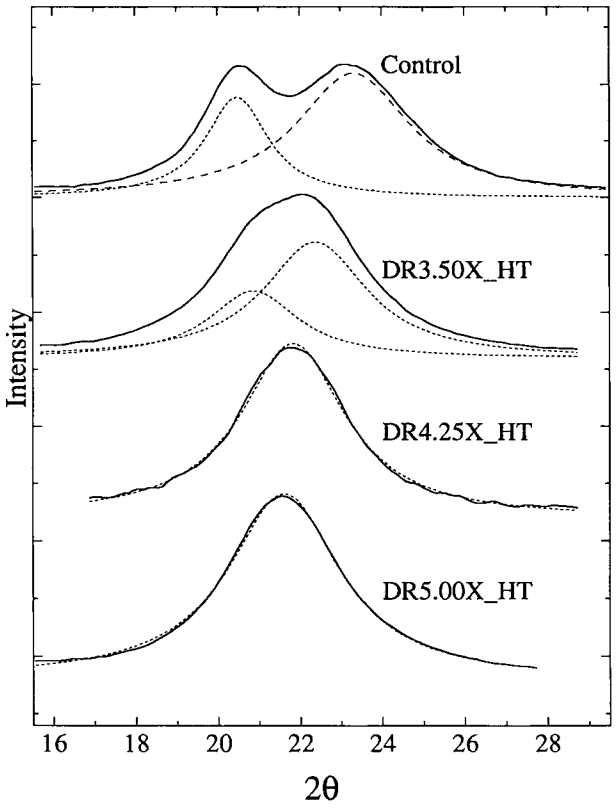

Figure 4 Equatorial profiles taken from WAXD images of the HT-drawing series (processing variables in Table I).

in the c-axis. As a result, the crystal cell density is lower under high draw ratios. Perhaps this suggests that the recrystallization process after partial melting (by the hot shoe) occurs with greater difficulty under high draw ratios. The equatorial peak positions from the on-line images, listed in Table II, are quite different from those observed from the off-package measurement.

Figure 5 shows equatorial scans from the images taken in the let-down experiments (LD series, Table I). Two reflection peaks (indicated by two dashed lines) are identifiable in all of the scans, which is consistent with the argument of a triclinic cell near room temperature. Notwithstanding that temperature at the detection spot is about constant (near room temperature), we found that the separation of the two peaks is generally smaller at high draw ratios (Table II). The merging of the two strong equatorial reflections also indicates the decrease in crystal density. This shows an implication similar to our earlier argument, i.e., if the hot shoe (200°C) provides a partial melting to the fibers, the high draw ratio has somewhat hindered the recrystallization process of some molten species.

The values of the Hermans orientation factor (f) for different equatorial reflections under different processing conditions are also listed in Table II. These values are calculated from the azimuthal scans [$I(\phi)$ vs. ϕ] taken at the diffraction maxima. Typical azimuthal scans of the 010/110 doublet during the let-down experiments are shown in Figure 6. In Table II, the calculated factors are considered to be high, indicating that the orientation of the crystals is high during the measurements ($f = 1$ indicates a perfect orientation of the crystals, $f = 0$ indicates a random orientation). Furthermore, these factors appear to increase with draw ratio during both high temperature and let-down experiments. Considering that drawing decreases the crystal density but increases the crystal orientation factor in fibers, a reasonable molecular picture can be depicted to explain this process. It is conceivable that the hot shoe (set at 200°C) has imposed a partial melting of the crystals in fibers. In both experiments (HT and LD), as the draw ratio increases, the orientation of the residual crystals becomes high but the subsequent recrystallization occurs with difficulty, resulting in a relatively low crystal density.

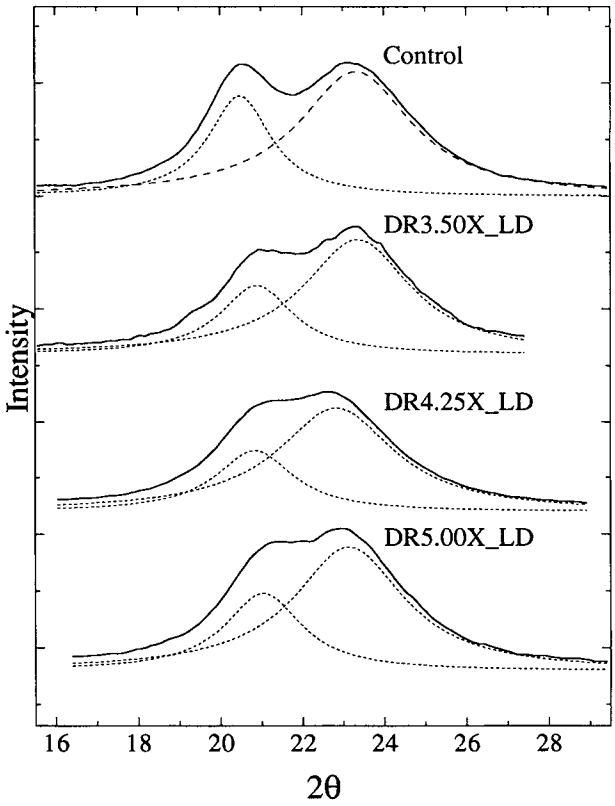

Figure 5 Equatorial profiles taken from WAXD images of the LD-drawing series (processing variables in Table I).

In contrast, as draw ratio decreases, the orientation of the residual crystals is low but the subsequent recrystallization during cooling can occur more readily, leading to a higher crystal density.

Spinning Experiment

During this measurement, the detection position was fixed at about 4 m from the spinneret. The WAXD images obtained under the two wind-up speeds (450 and 1,200 m/min) are very similar. A typical image taken at 1,200 m/min speed is shown in Figure 6. The quality of the images in this measurement is not as good as in the images taken in the drawing measurement for two reasons. 1) The crystallinity was low during spinning, which resulted in a lower scattering contrast and thus less diffraction signal. 2) The beamstop became misaligned during the measurement, which distorted the image in the equatorial direction (Fig. 6). In spite of the poor data quality, several unique features can still be identified from this image (Fig. 7). First, we find that all layer line reflections (002 and 015) are missing at a temperature (ca. 50°C) where crystallization is supposed to be completed. The only crystal signature observed here is the predominant crystal peak at 20.41° (2θ) that is superimposed with an amorphous phase with peak position at 19.81° (2θ). This feature is quite different from the image obtained from the off-package quenched fiber, which showed two strong equatorial reflection peaks at 20.94° and 22.62° and reflections along the 002 and 015 layer lines. Second, we find that both crystal and amorphous phases (during spinning) indicate some degrees of orientation (Fig. 7). The estimated Hermans orientation factors for the two phases are $f_{crystal} = 0.35$ and $f_{amorphous} = 0.15$. In fact, the observed on-line images during the spinning experiment are very similar to the ones we obtained during synchrotron X-ray measurements.[22] In the synchrotron measurement, we find that the predominant feature

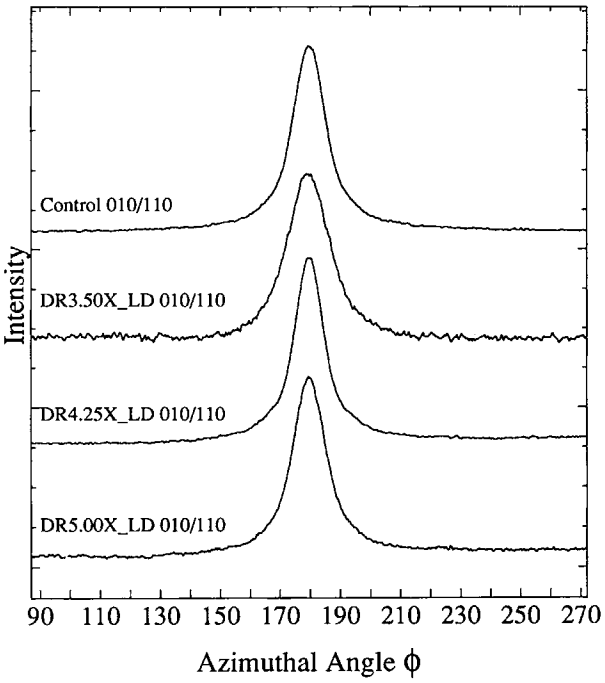

Figure 6 Azimuthal scans [$I(\phi)$ vs. ϕ] taken at the maximum of the 010/110 doublet during the let-down experiments.

Table II 2θ Positions and Hermans Orientation Factors (f)[a] of Strong Reflections at the Equator from On-Line Measurements vs. Off-Package Measurements

Item	Control	3.50×_HT	4.25×_HT	5.00×_HT	3.50×_LD	4.25×_LD	5.00×_LD
On-Line							
100	20.49	20.83			20.94	20.83	21.05
010/110	23.28	22.40			23.39	22.84	23.17
100/010/110			21.84	21.62			
f_{100}	0.69				0.68	0.82	0.81
$f_{010/110}$	0.80	0.81			0.76	0.84	0.87
$f_{100/010/110}$			0.84	0.83			
Off-Package							
100	20.57	20.75	20.71	20.71	—	20.67	20.82
010/110	23.21	23.18	22.97	22.82	—	22.92	22.98

[a] $$f = \frac{3 < \cos^2 \phi > -1}{2} \quad < \cos^2 \phi > = \frac{\int_0^{\pi/2} I(\phi) \sin \phi \cos^2 \phi d\phi}{\int_0^{\pi/2} I(\phi) \sin \phi d\phi}$$

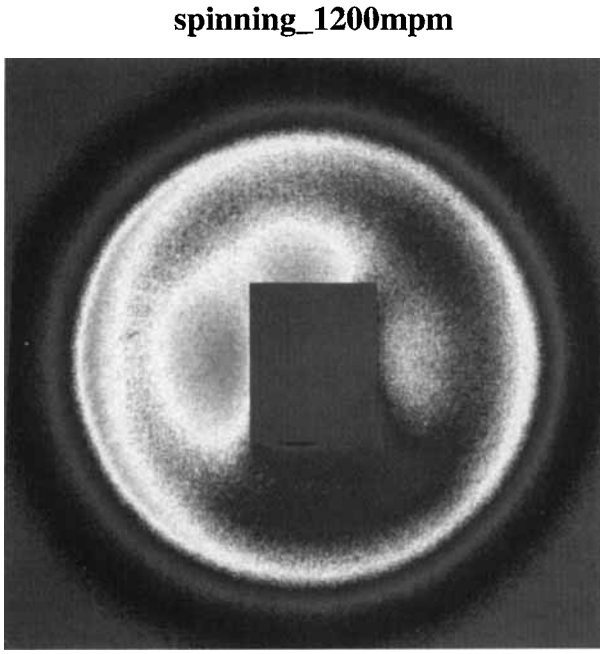

Figure 7 On-line WAXD image taken during melt spinning measurement with 1,200 m/min take-up speed.

for the crystal phase is the appearance of the 100/010/110 triplet peak, conventionally indicating a pseudohexagonal crystal cell above the Brill transition temperature. Since we have never observed the reflections at other layer lines during spinning at wind-up speeds up to 3,000 m/min, we believe that the crystals developed during spinning are two dimensional in nature with a hydrogen-bonding characteristic. It may be considered as a mesomorphic phase comprising well-defined hydrogen-bonding sheets.

Path Forward for the On-Line Setup

In order to successfully apply the on-line X-ray diffraction technique to monitor structural changes for different processes, several points of caution and potential improvement will be addressed in this section. The first concern is the choice of proper image plate system. In this demonstration, we selected the Fuji™ system because of the availability. However, this is not the most suitable choice because the Fuji™ scanner requires the scanning of an entire plate. Using a resolution of 100 mm, each scanning has generated a binary file of 10 MB that is cumbersome to be analyzed by most desk-top personal computers. In our setup, we have rotated the image plate to acquire four images. The effective size of each image is about 1.5 MB, which is more convenient for the analysis. This can be accomplished by the use of a small image plate. In this case, the Phosphorimager scanning device manufactured by Molecular Dynamics™, which can scan the plate of any reduced size, is suitable.

It is imperative to note that the phosphor imaging plate is susceptible to all energies (wavelengths) from the X-ray source. This is evident by the equatorial streaks observed in Figures 3 and 6. It is possible that some broadening may occur in the equatorial reflections or the streaks may superimpose with the reflections (although these are not seen in this work). If these problems become severe, a monochromator has to be installed to eliminate the white radiation. In most cases, this will not be a preferred arrangement because the X-ray intensity would be significantly reduced by the monochromator, resulting in a much longer collection time. Furthermore, we believe that a small X-ray source is much more easily incorporated in the design of an on-line setup (with less bulky transformer and cooling systems).

It is also important to note that the exposed image on the image plate has a limited shelf time. This is due to the self-deexcitation of the phosphor molecules and self-exposure due to natural radioactivity (cosmic rays and surrounding materials). The scanning of an image plate after 10 h of storage time only yields 50% of the original intensity. The exposure of a plate for over 24 h of storage time is practically of little use.[23]

The arrangement of X-ray collimator, fiber guide, beamstop(s), and detection plate holder is the most critical part of the on-line setup design. It has to be designed so as to accomplish the following objectives. 1) The safety concern around the use of an open X-ray beam in a plant or laboratory environment has to be resolved satisfactorily by incorporating a suitable shield, as well as restricting access to the area while the shutter is open. 2) The fiber guide should be positioned only to stabilize the sample in front of the X-ray beam without modifying the structure by snubbing or friction. 3) The sample-to-detector distance should be fixed for all measurements. 4) The center of the beam should also be fixed and maintained aligned with respect to the beam stop. In practice, this arrangement can be an integrated into a "detection head" and mounted on a mechanical arm with many degrees of freedoms (translational and rotational). In this case, it can be fitted to some hard-to-reach positions during the fiber process.

CONCLUSIONS

In this work, we demonstrate that a simple on-line X-ray detection system can be used to monitor structural changes during different fiber processing. The key to the design is the use of a phosphor image plate for X-ray detection, which provides not only excellent sensitivity but also good dynamic range in the data. In the two chosen fiber processes, post-drawing and melt spinning, we observed significant structural differences between the on-line measurement and the off-package measurement from the quenched samples. It is concluded that the high draw ratio can hinder the subsequent recrystallization process but impose a high orientation on the residual crystals. During spinning, the crystal formation is predominantly two dimensional in nature, having a hydrogen-bonding characteristic. Finally, we have discussed several ways to improve the design to a more versatile on-line X-ray setup and noted some points of caution for the application.

We thank Dr. Alan D. Kennedy of DuPont CR&D for helpful technical suggestions and comments on the data analysis. The design of the on-line apparatus was assisted by Larry Rock Automation Associates, who kindly provided Figure 1. B. S. H. acknowledges the partial financial support of this project by NSF-GOALI program (DMR 9629825).

REFERENCES

1. L. E. Alexander, *X-Ray Diffraction Methods in Polymer Science,* R. E. Krieger Pub., Malabar, FL, 1985.
2. S. J. Balta-Calleja and C. J. Vonk, *X-Ray Scattering of Synthetic Polymers,* Elsevier, New York, 1989.
3. F. Chappel, M. Culpin, R. Gosden, and T. Tranter, *J. Appl. Chem.,* **14,** 12 (1964).
4. K. Katayama, T. Amano, and K. Nakamura, *Kolloid Z. Z. Polym.,* **226,** 125 (1968).
5. J. R. Dees and J. E. Spruiell, *J. Appl. Polym. Sci.,* **18,** 1055 (1974).
6. J. Spruiell and J. White, *Polym. Eng. Sci.,* **15,** 660 (1975).
7. H. Nadella, H. M. Henson, J. E. Spruiell, and J. L. White, *J. Appl. Polym. Sci.,* **21,** 3013 (1977).
8. V. Bankar, J. E. Spruiell, and J. L. White, *J. Appl. Polym. Sci.,* **21,** 2341 (1977).
9. M. D. Danford, J. E. Spruiell, and J. L. White, *J. Appl. Polym. Sci.,* **22,** 3315 (1978).
10. H. Haberkorn, K. Hahn, H. Breuer, H. D. Dorrer, and P. Matthies, *J. Appl. Polym. Sci.,* **47,** 1551 (1993).
11. H. Breuer, H. Haberkorn, K. Hahn, and P. Matthies, *Chemiefasern/Textilindustrie,* **42/94,** 662 (1992).
12. J. Miyahara, *Chemistry Today,* **223,** 29 (1987).
13. Y. Amemiya, Y. Satow, T. Matsushita, J. Chikawa, K. Wakabayashi, and J. Miyahara, *Topics Curr. Chem.,* **147,** 121 (1988).
14. W. Hillen, U. Schiebel, and T. Zaengel, *Med. Phys.,* **14,** 744 (1987).
15. H. von Seggern, *Nucl. Instrum. Methods,* **A323,** 467 (1992).
16. M. W. Tate, E. F. Eikenberry, S. L. Barna, M. E. Wall, J. L. Lowrance, and S. M. Gruner, *J. Appl. Cryst.,* **28,** 196 (1995).
17. B. Rodricks, R. Clarke, R. Smither, and A. Fontaine, *Rev. Sci. Instrum.,* **60,** 2586 (1989).
18. M. Stanton, W. C. Phillips, D. O'Mara, I. Naday, and E. Westbrook, *Nucl. Instrum. Methods,* **A325,** 558 (1993).
19. R. Brill, *J. Prakt. Chem.,* **161,** 49 (1943).
20. C. W. Bunn and E. V. Garner, *Proc. Roy. Soc.,* **A189,** 39 (1947).
21. B. S. Hsiao and A. D. Kennedy, to appear.
22. A. D. Kennedy, B. S. Hsiao, R. A. Leach, R. Barton, S. Seifert, and H. G. Zachmann, to appear.
23. F. Ne, D. Gazeau, J. Lambard, P. Lesieur, and T. Zemb, *J. Appl. Cryst.,* **26,** 763 (1993).

Received January 31, 1996
Accepted July 25, 1996